AIP | Review of Scientific Instruments

Cold testing of quasi-optical mode converters using a generator for non-rotating high-order gyrotron modes

S. G. Kim, D. S. Kim, M. S. Choe, W. Lee, J. So, and E. M. Choi

Citation: Review of Scientific Instruments **85**, 104709 (2014); doi: 10.1063/1.4898180

View online: http://dx.doi.org/10.1063/1.4898180

View Table of Contents: http://scitation.aip.org/content/aip/journal/rsi/85/10?ver=pdfcov

Published by the AIP Publishing

Cold testing of quasi-optical mode converters using a generator for non-rotating high-order gyrotron modes

S. G. Kim,[1] D. S. Kim,[2] M. S. Choe,[2] W. Lee,[3] J. So,[3] and E. M. Choi[1,2,a)]
[1]*School of Electrical and Computer Engineering, Ulsan National Institute of Science and Technology (UNIST), Ulsan 689-798, South Korea*
[2]*Physics Department, Ulsan National Institute of Science and Technology (UNIST), Ulsan 689-798, South Korea*
[3]*Agency for Defense Development (ADD), Daejeon 305-152, South Korea*

(Received 3 July 2014; accepted 4 October 2014; published online 27 October 2014)

In this paper, we test the performance of a quasi-optical, internal-gyrotron mode converter. When cold testing mode converters, a rotating higher-order mode is commonly used. However, this requires a nontrivial design and precise alignment. We thus propose a new technique for testing gyrotron mode converters by using a simple, non-rotating, higher-order mode generator. We demonstrate the feasibility of this technique for a W-band gyrotron quasi-optical mode converter by examining the excitation of a $TE_{6,2}$ mode from a non-rotating mode generator. Our results demonstrate that this new cold-test scheme is an easy and efficient method for verifying the performance of quasi-optical mode converters. © *2014 AIP Publishing LLC*. [http://dx.doi.org/10.1063/1.4898180]

I. INTRODUCTION

The gyrotron is a fast-wave vacuum device capable of generating hundreds of kilowatts of electromagnetic power in the millimeter and sub-millimeter wave range[1–5] and has emerged as an excellent radio frequency (RF) power source for applications such as plasma heating in fusion devices, dynamic nuclear polarization (DNP), nuclear magnetic resonance (NMR), environmental monitoring, and so on.[6–10] The gyrotron consists of several major components including a magnetron injection gun (MIG), open-ended cavity, mode converter, and collector.[11–13] The mode converter is critical: it converts a higher-order mode from the interaction circuit into a Gaussian-like beam, which effectively transmits RF power through free space.[14–16]

Typically, a quasi-optical mode converter (QOMC) comprises an open-ended, non-symmetrical waveguide launcher and a series of quasi-parabolic mirrors, which are situated directly after the gyrotron's interaction circuit.[17] A QOMC must be tested before being positioned in the vacuum tube, owing to the following issues: First, there may be inaccuracies in the location and alignment of mirrors, which must be resolved in air before the QOMC is placed in vacuum. Second, the RF beam size should be measured accurately as it propagates in space, in order to correctly design transmission-line components after the gyrotron. Finally, but most importantly, the quality of the generated output beam should be compared to the calculated beam quality to measure how well the launcher and mirrors are fabricated.

To the best of our knowledge, all reported QOMCs have been tested using rotating-mode generators, which theoretically produce real operating cavity modes (rotating higher-order modes). While this method is seemingly ideal, fabricating a rotating-mode generator (RMG) for cold testing is problematic. First, RMGs require a demanding design process for exciting a target mode. Then, even if the design and fabrication of the mode generator is carried out properly, generating a desired rotating mode requires numerous iterations in actual experiments to fully align the system, since the mode-generator components are very sensitive to the beam-propagation alignment. Additionally, the generated rotating mode may not be ideal, possibly containing mixed modes due to a combination of problems such as misalignment of the mode generator and poor joint assembly between the mode generator and the mode converter, which may predominantly affect the mode-converter's efficiency.

The purpose of QOMC cold testing is to check whether the output beam is well matched with the as-designed beam. Therefore, instead of using a rotating $TE_{m,p}$ mode generator for testing the QOMC, we propose the use of a compact, non-rotating, higher-order $TE_{m,p}$ mode generator, which is much easier to design and does not require alignment. If one can predict an output-beam pattern from a QOMC excited by a non-rotating mode generator (NRMG)—by comparing cold tests with simulation—the efficiency of the QOMC can be estimated. In this paper, we propose a test scheme using a $TE_{6,2}$ NRMG for a W-band gyrotron QOMC. The proposed scheme is compared to the existing scheme, which uses a rotating $TE_{6,2}$ mode generator, and the feasibility of the proposed method is then discussed.

This paper is organized as follows: The theory of the mode converter and system setup for the cold test are presented in detail in Sec. II. In Sec. III, the experimental results for the cold tests using the NRMG and RMG are presented and compared with simulation. Finally, we present our conclusions in Sec. IV.

II. EXPERIMENTAL SETUP

In this section, we explain the experimental setup for testing a QOMC using a NRMG. In Sec. II A, we introduce the

a)Author to whom correspondence should be addressed. Electronic mail: emchoi@unist.ac.kr

basic scheme and design parameters for the mode converter used for the cold test. In Sec. II B, the design of a higher-order NRMG and the cold-test experimental setup are presented in detail.

A. Theory of mode converters

Most current high-power gyrotrons use an internal QOMC to convert a high-order mode excited in an interaction circuit into a Gaussian beam at the output window. We designed a four-mirror internal QOMC that consists of a dimpled-wall helical launcher and a series of mirrors. The dimpled-wall helical launcher is the first component of the internal QOMC.[18–20] The beam radiating from the launcher passes through the mirrors, producing the desired Gaussian-like beam. The beam from the dimpled-wall helical launcher diverges when it propagates, and the first mirror is designed for beam convergence using a quasi-parabolic equation. The profile of the quasi-parabolic mirror is given by

$$\begin{aligned} x &= 2f_p \tan\left(\frac{\varphi}{2}\right) + r_{caustic}\left[1 + \varphi \tan\left(\frac{\varphi}{2}\right)\right] \\ y &= f_p\left[\tan^2\left(\frac{\varphi}{2}\right) - 1\right] \\ &\quad + r_{caustic}\left[\frac{\varphi}{2}\tan^2\left(\frac{\varphi}{2}\right) + \tan\left(\frac{\varphi}{2}\right) - \frac{\varphi}{2}\right], \end{aligned} \tag{1}$$

where f_p denotes the focal length of the parabolic mirror. The caustic radius $r_{caustic}$ is given by

$$r_{caustic} = \frac{m}{k_\perp} = r_{wg}\frac{m}{\nu'_{mp}}, \tag{2}$$

where $k_\perp$ is the transverse wave number of beam, m is the azimuthal mode index, r_{wg} is the radius of the cylindrical waveguide, and ν'_{mp} is the pth non-vanishing zero of the derivative of the Bessel function $J'_m(x)$. In Eq. (1), φ denotes the azimuthal bounce angle, defined as

$$\varphi = \arccos\left(\frac{m}{\nu'_{mp}}\right). \tag{3}$$

A summary of the design parameters of an optimized dimpled-wall helical launcher is given in Table I. Using the above equations and design parameters, we designed two different sets of mode converters using the commercially available Surf3d code (Lexam Research).[21] The first mode converter, shown in Fig. 1(a), is designed for a 160-mm smooth launcher with three mirrors, and the second mode converter, shown in Fig. 1(b), is optimized for a 65.4-mm dimpled launcher with four mirrors. In Fig. 1, the blue arrow indicates the beam path generated from the launcher, and the ruler is in centimeters.

TABLE I. Critical design parameters for the mode converter.

Frequency	W band
Operating mode	$TE_{6,2}$
Radius of the launcher	7 mm
Length of the launcher	65.4 mm
Cut length of the launcher	23 mm
Number of mirrors	4

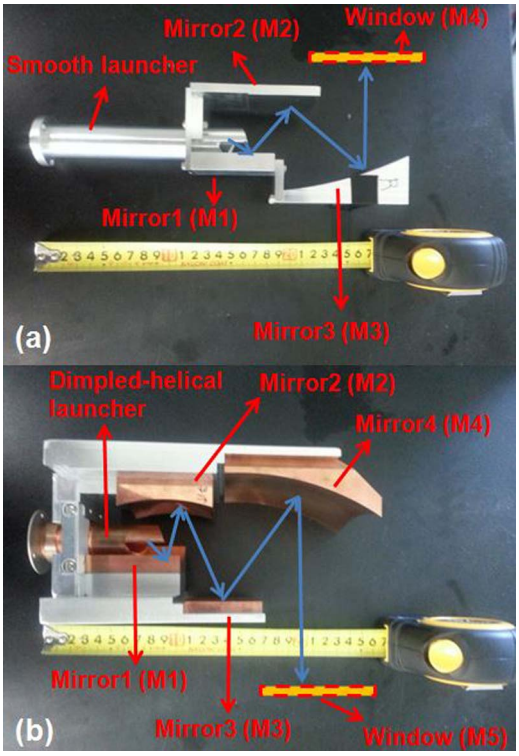

FIG. 1. Fabricated mode converters: (a) A mode converter with three parabolic mirrors and a 160-mm smooth launcher. (b) A mode converter with four parabolic mirrors and a 65.4-mm dimpled launcher.

B. Higher-order non-rotating mode generator

A $TE_{6,2}$ NRMG has a simple cavity shape, as shown in Fig. 2. A summary of the design parameters for the mode-generator cavity is given in Table II. The down-taper section in Fig. 2, denoted by L_1, is a cutoff section that prevents the reflected RF power from reaching the gun. In the uniform middle section, denoted by L_2, the target mode is excited. The proposed mode generator excites only the linear $TE_{m,p}$ mode, unlike typical mode generators that produce rotating $TE_{m,p}$ modes. Fig. 3 shows the fabricated $TE_{6,2}$ NRMG using the cavity parameters listed above. The connections of the mode-generator cavity are designed to minimize unwanted mode generation at sharp edges.[22–24] The inner rod is inserted at the center of the mode-generator cavity in order to prevent excitation of neighboring modes, with a WR08 waveguide

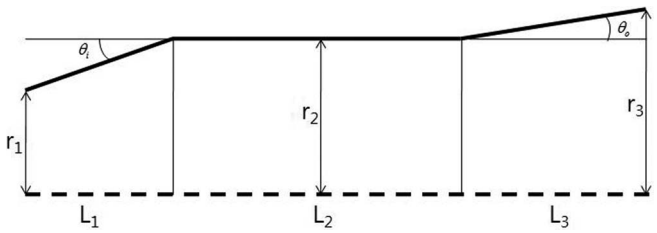

FIG. 2. Internal geometric profile of a non-rotating mode-generator (NRMG) cavity.

TABLE II. Design parameters for the cavity resonator.

Operating frequency	95.15 GHz
Diffractive Q factor	893
Input taper radius(r_1)	5.773 mm
Cavity radius(r_2)	5.895 mm
Output taper radius(r_3)	7.0 mm
Input taper section length(L_1)	9.551 mm
Cavity section length(L2)	18.0 mm
Output taper section length(L_3)	53.549 mm

attached to directly feed the desired frequency. The fabricated NRMG was thus expected to generate a high-purity linear $TE_{6,2}$ mode.[25,26]

Fig. 4 shows the experimental setup for cold testing the mode-converter systems. The higher-order $TE_{6,2}$ NRMG is connected directly from the source of a vector network analyzer (VNA) WR08 waveguide and feeds the launcher of the mode converter. The full system is mounted on an optical table and each component can be adjusted with an *x*-*y*-*z* stage controller. The cold test was conducted using an Agilent VNA (PNA-X5247A) with OML WR08 extenders for both the transmitter and receiver. In particular, one WR08 extender is used as a transmitting source and is connected to the mode generator, while the other open-ended metallic WR08 waveguide probes the field pattern in free space. The field pattern is scanned at the planes from each mirror, as indicated in Fig. 1. The surrounding environment was properly covered with eccosorb (AEMI AEC-1.5) to minimize unwanted field interference.

To compare the performance of the proposed NRMG, we tested the mode-converter systems using both NRMGs and RMGs. We further used the 65-mm dimpled launcher, the 90-mm dimpled launcher, and the 160-mm smooth launcher for a feasibility test using the NRMG.

III. EXPERIMENTAL RESULTS AND DISCUSSIONS

A. Measurement results using NRMG

Fig. 5 shows a field scan from the fabricated NRMG compared to the theoretically calculated field pattern of the $TE_{6,2}$ mode result. The calculated field pattern assumes that the cavity structure is a cylinder with a constant radius of 5.895 mm in order to produce the correct resonant frequency for the system. In the experiment, however, the actual cavity has a

FIG. 3. Assembly of a fabricated NRMG.

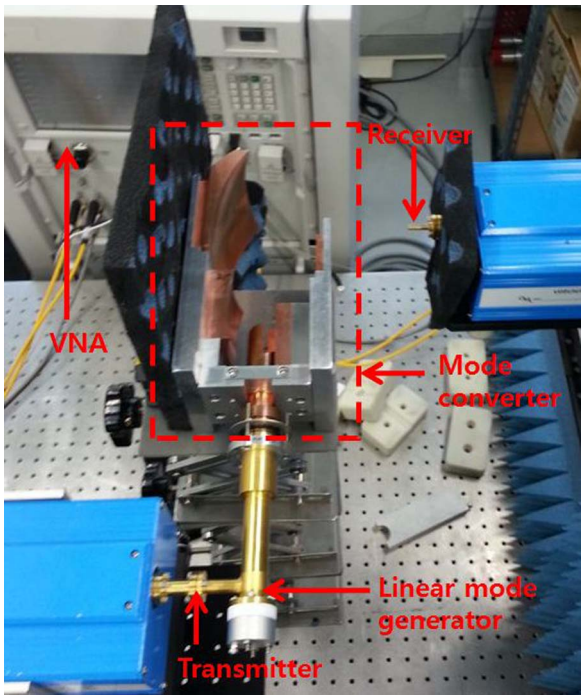

FIG. 4. Experimental setup for the cold test of the mode-converter system using a NRMG.

radially increasing tapered section whose final radius at the aperture is 7 mm. Here, the field is scanned at a location approximately 1 mm from the aperture of the mode-generator cavity so that the scanned region of in-radius field propagation is greater than 7 mm. For this reason, the measured field pattern shows greater intensity in the second radial peak than the first radial peak, since a secondary radial-field intensity increases proportionally with geometric radius. Moreover, diffraction and scattering between the metal components in the mode generator and detector probe resulted in blurry field images. Although it is hard to prove the measured field pattern's $TE_{6,2}$ signature quantitatively, owing to the reasons mentioned above, the generated mode distinctively shows six azimuthal and two radial variations, which confirms $TE_{6,2}$ mode generation. To examine the feasibility of the proposed technique, we used three sets of mode converters containing different launchers to provide proof-of-principle tests using well-controlled independent test systems. These three systems

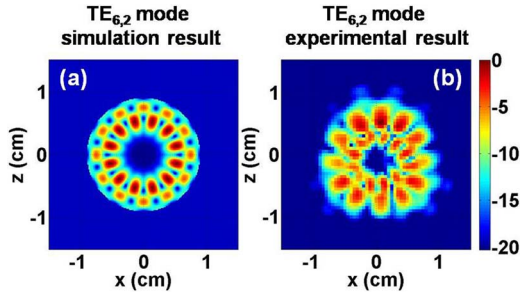

FIG. 5. $TE_{6,2}$ mode plot: (a) The calculated $TE_{6,2}$ mode-pattern plot. (b) The measured $TE_{6,2}$ mode pattern from the NRMG.

are driven by the $TE_{6,2}$ NRMG and the standard $TE_{6,2}$ RMG, using the following three setups:

(A) Desired quasi-optical system (the optimized QOMC system for rotating $TE_{6,2}$ mode): 65.4 mm dimpled launcher + 4 mirrors
(B) Undesired quasi-optical system 1 (a poor quality dimpled-wall launcher is used on purpose): 90 mm dimpled launcher + 4 mirrors
(C) Undesired quasi-optical system 2 (smooth launcher is chosen): 160 mm smooth launcher + 3 mirrors

Test system (A) should give the most-Gaussian beam pattern at the final location of the mode converter if the rotating $TE_{6,2}$ mode drives the launcher. Test system (B) and (C) are chosen to verify that our proposed scheme works with undesired mode converters. The NRMG and RMG are compared in simulation and experiment. The field-scan results from the experiment for test system (A) are shown and compared to simulation results in Fig. 6. Here, the measured electric-field intensity at each plane shows a good agreement with the simulation.

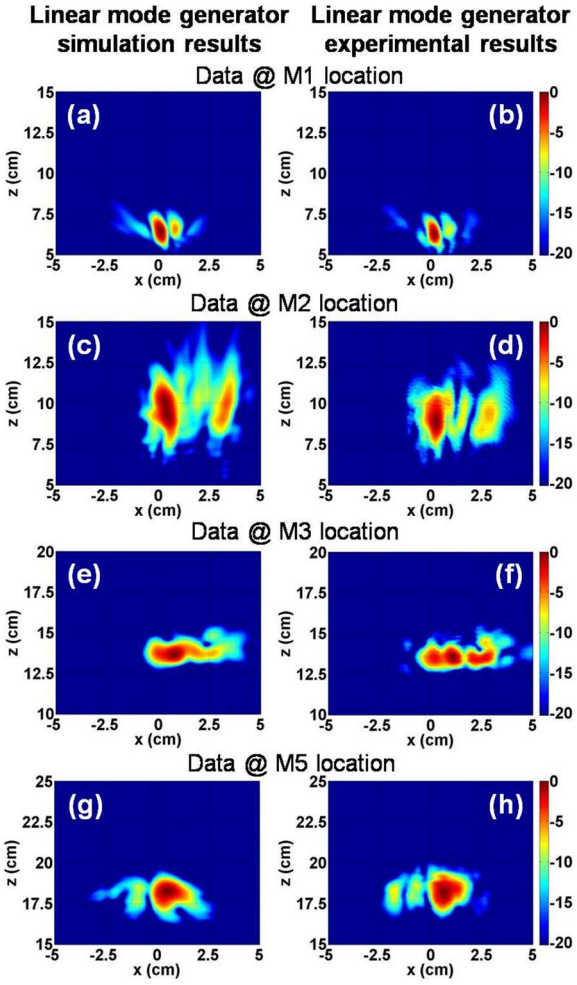

FIG. 6. (a), (c), (e), (g): Simulation results for the 65.4-mm dimpled launcher using the $TE_{6,2}$ NRMG at different locations. (b), (d), (f), (h): Experimental results for the 65.4-mm dimpled launcher using the $TE_{6,2}$ NRMG at different locations. The measurement locations M1, M2, M3, and M5 are shown in Fig. 1(b). The CCF values between (a) and (b), (c) and (d), (e) and (f), and (g) and (h) are 98.9%, 97.2%, 97.9%, and 97.2%, respectively.

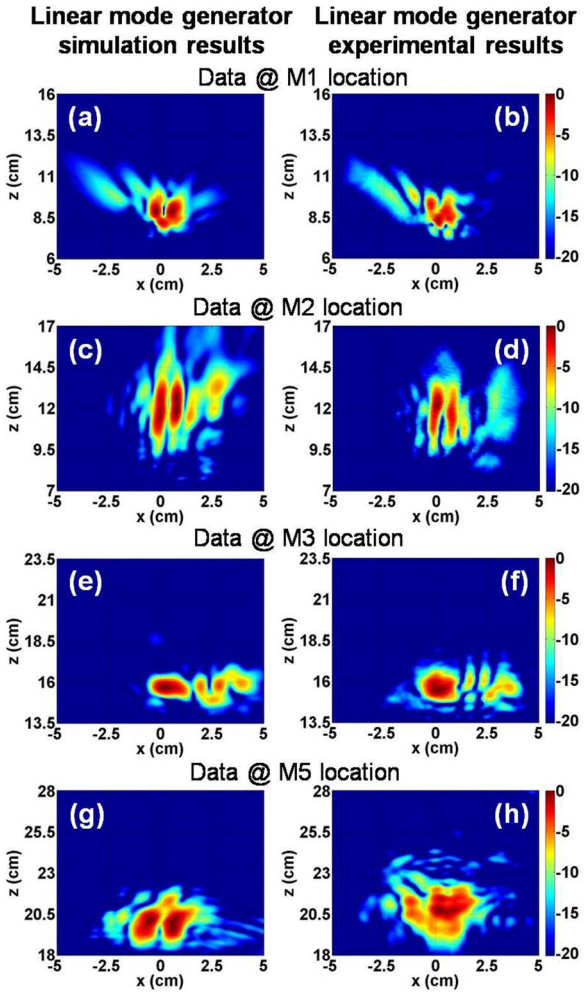

FIG. 7. (a), (c), (e), (g): Simulation results for the 90.0-mm dimpled launcher using the $TE_{6,2}$ NRMG. (b), (d), (f), (h): Experimental results for the 90.0-mm dimpled launcher using the $TE_{6,2}$ NRMG. The measurement locations M1, M2, M3, and M5 are shown in Fig. 1(b). The CCF values between (a) and (b), (c) and (d), (e) and (f), and (g) and (h) are 98.2%, 96.4%, 97.2%, and 95.2%, respectively.

Fig. 7 summarizes the field-scan data from the experimental test system (B) compared to the simulation results. This test system also shows a very good agreement between simulation and experiment, even though the 90-mm dimpled launcher is not optimized. The results of test system (C) are plotted in Fig. 8. Again, though test system (C) has a non-optimized smooth 160-mm launcher, the field prediction from each plane agrees with the experimental data very well. The experimental test systems (A), (B), and (C) demonstrate that when the designed mode converter is driven by a NRMG, the performance of the mode converter can be quantified by comparing experiment and simulation. This was accomplished using both sets of amplitudes and phases in a cross-correlation function (CCF),

$$CCF = \sum_{i,j} u_{\exp} e^{j\varphi} \cdot (u_{simul} e^{-j\varphi'})^* = \sum_{i,j} |u_{\exp}| \cdot |u_{simul}| e^{j(\varphi-\varphi')}, \quad (4)$$

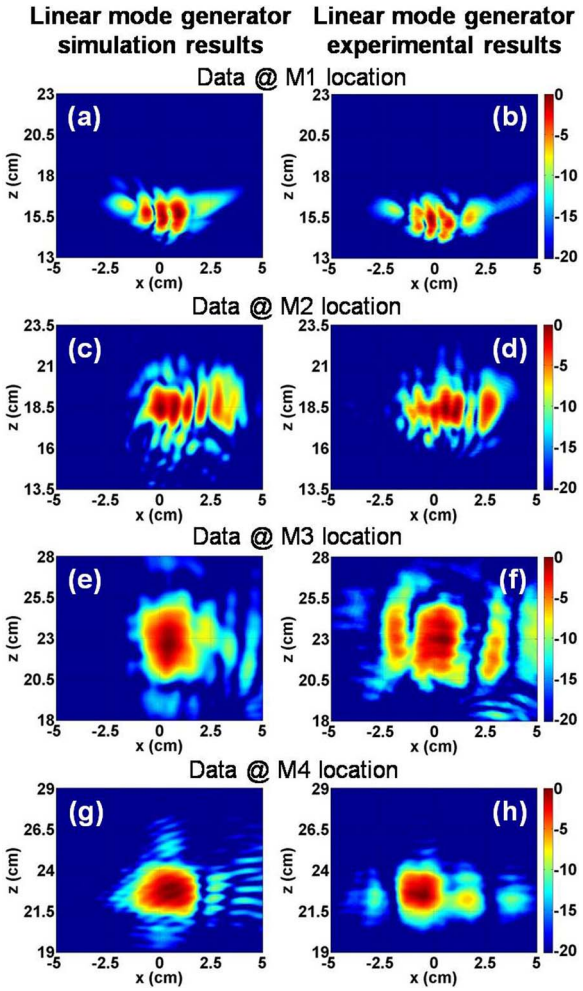

FIG. 8. (a), (c), (e), (g): Simulation results for the 160-mm smooth launcher using the $TE_{6,2}$ NRMG. (b), (d), (f), (h): Experimental results for the 160-mm smooth launcher using the $TE_{6,2}$ NRMG. The measurement locations M1, M2, M3, and M4 are shown in Fig. 1(a). The CCF values between (a) and (b), (c) and (d), (e) and (f), and (g) and (h) are 97.9%, 96.4%, 91.8%, and 95.4%, respectively.

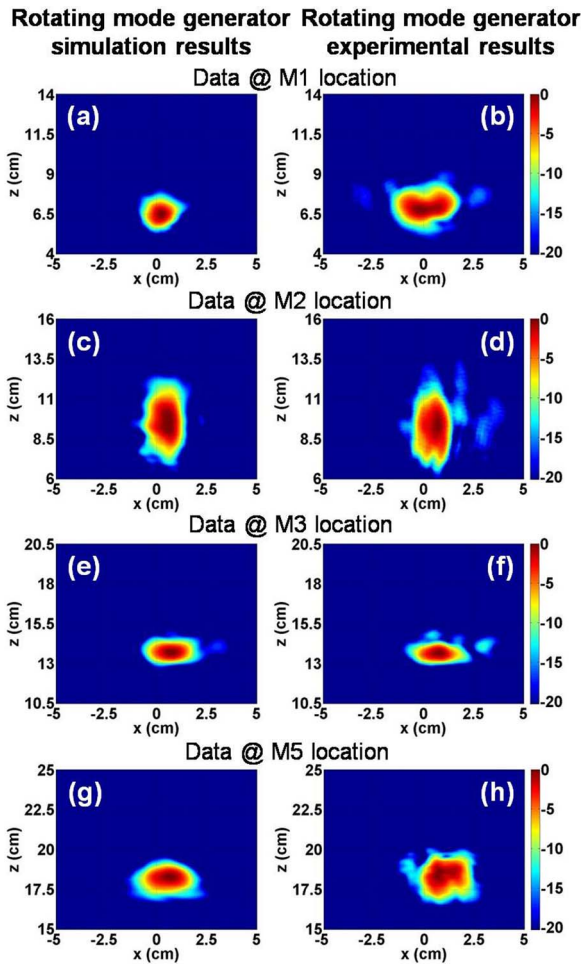

FIG. 9. (a), (c), (e), (g): Simulation results for the 65.4-mm dimpled launcher using the $TE_{6,2}$ RMG. (b), (d), (f), (h): Experimental results for the 65.4-mm dimpled launcher using the rotating $TE_{6,2}$ mode generator. The measurement locations M1, M2, M3, and M5 are shown in Fig. 1(b). The CCF values between (a) and (b), (c) and (d), (e) and (f), and (g) and (h) are 97.6%, 97.5%, 97.9%, and 97.7%, respectively.

where $|u_{\text{exp}}|$ and $|u_{simul}|$ are the moduli of the normalized experimentally measured field coefficient and the normalized simulation field coefficient, respectively, and φ and φ' are the phases of the experimental measured field coefficient and the simulation field coefficient, respectively. The CCFs for the test systems are calculated and indicated in the captions of Fig. 6–8, and all results show excellent agreement between experiment and simulation, with CCF values greater than 95%.

B. Measurement results using RMG

To compare the validity of the mode-converter test using the $TE_{6,2}$ NRMG, we used a standard mode-converter setup using a $TE_{6,2}$ RMG.[27,28] Similar to Sec. III A, we tested system (A) for the 65.4-mm dimpled launcher and system (C) for the 160-mm smooth launcher. System (B) was not tested due to difficulties in building a connector between the RMG and the 90-mm dimpled launcher. Fig. 9 shows the experimental results for test system (A) using the RMG with the 65.4-mm dimpled launcher. The output field pattern for the last mirror shows a well-shaped Gaussian beam in simulation. The experimental results were compared to the simulation results, and the CCF values for all planes are above 97%.

Test system (C) was also measured using the $TE_{6,2}$ RMG, and the measured field patterns agree well with the simulation, with CCF values greater than 95%, as shown in Fig. 10. Comparing the experimental data and the simulated field prediction, the test results using the NRMG are on par with those using the RMG. The CCF values comparing simulation and experiment at the window location are summarized in Table III for all three test systems, using both NRMGs and RMGs. As shown in Table III, all results show excellent agreement between experiment and simulation at the window plane, with CCF values above 95%; there is negligible difference in CCF values between the NRMG and RMG cases.

In order to check for discrepancies between the CCF values of the measured and simulated field patterns, we performed additional simulations to imitate the real experimental setup. Up to this point, all simulations using the NRMG and the RMG assumed that the ideal $TE_{6,2}$ mode was

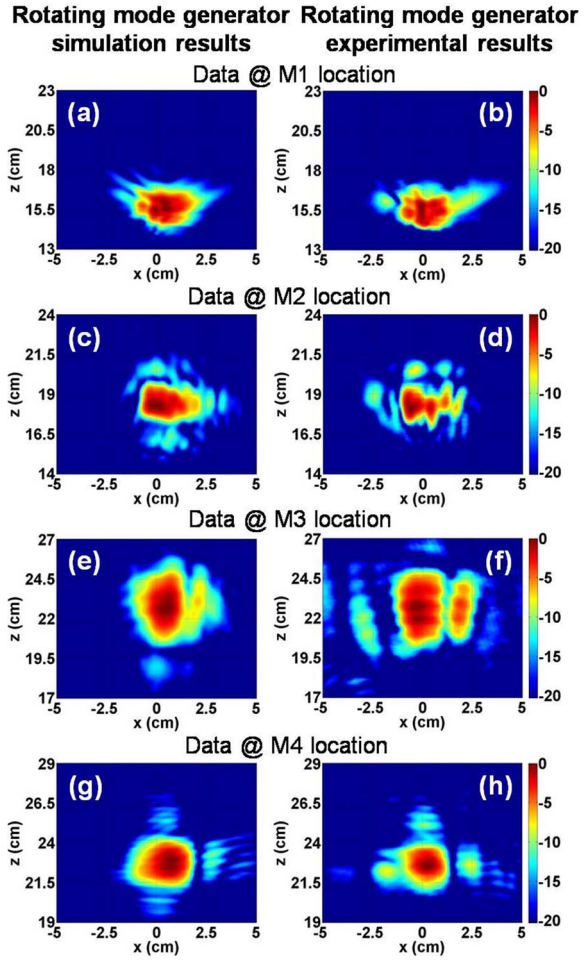

FIG. 10. (a), (c), (e), (g): Simulation results for a 160-mm smooth launcher using the $TE_{6,2}$ RMG, (b), (d), (f), (h): Experimental results for a 160-mm smooth launcher using the $TE_{6,2}$ RMG. The measurement locations M1, M2, M3, and M4 are shown in Fig. 1(a). The CCF values between (a) and (b), (c) and (d), (e) and (f), and (g) and (h) are 97.6%, 96.9%, 92.4%, and 95.7% respectively.

TABLE III. Summary of the quantitative comparison between the simulation and the experiment (CCF values at the window location).

	System (A)	System (B)	System (C)
Non-rotating mode generator	97.2%	95.2%	95.4%
Rotating mode generator	97.7%	N/A	95.7%

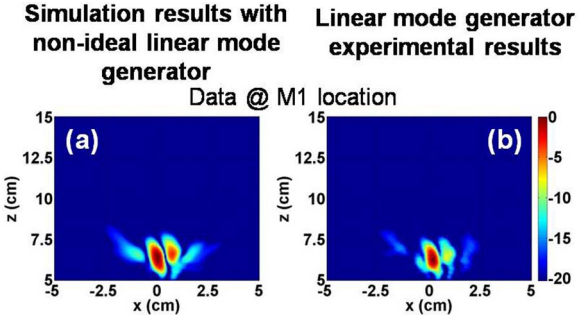

FIG. 11. (a) The simulation result of the mode-mixed $TE_{6,2}$ NRMG using the 65.4 mm dimpled launcher (b) The measured field pattern of the 65.4 mm dimpled launcher. The CCF between (a) and (b) is 98.8%.

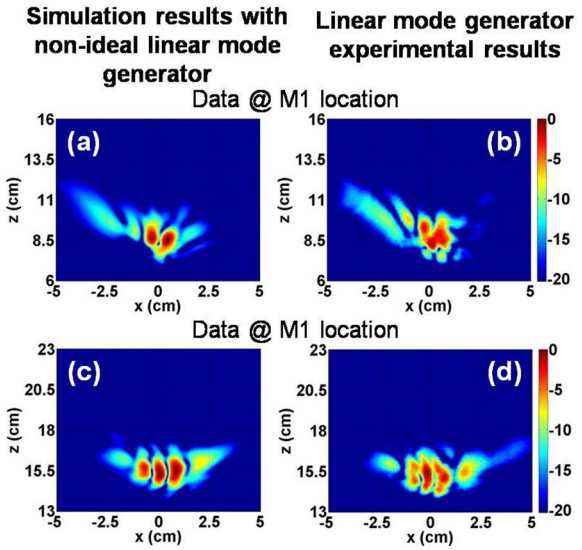

FIG. 12. (a) and (c) The simulation results of the mixed $TE_{6,2}$ NRMG using the 90.0-mm and the 160-mm launcher, respectively. (b) and (d) The measurement results of the 90.0-mm and 160-mm launcher, respectively. The CCF between (a) and (b), and (c) and (d) are 97.8% and 98.1%, respectively.

generated. However, the constructed mode generators contain imperfections, which result in unwanted modes that are excited simultaneously with the desired mode. Moreover, the mode generator and the quasi-optical launcher may be slightly misaligned due to an imperfect joint assembly. We analyzed the simulation results by allowing mode mixtures and misalignment of the structure during mode generation, so that the simulated data show strong agreement with experiment. The simulation in Fig. 11 is the result for test system (A) using a counter-clockwise, rotating $TE_{6,2}$ mode, mixed with the linear $TE_{6,2}$ mode by forced misalignment of the structure. In this case, about 5.3% of the counter-clockwise $TE_{6,2}$ mode power is mixed with about 94.7% of the linear $TE_{6,2}$ mode power. Compared to Fig. 6, the results from the mixed-mode generator show much better agreement with experiment, with a CCF value greater than 98%. Likewise, simulations considering mode mixing and misalignment in test systems (B) and (C) were compared to the experimental data at the plane just off the launcher tip, as shown in Fig. 12. These results are also in much better agreement, with the CCF as high as 98%. From this analysis, we conclude that mixed-mode generations, along with misalignment of the mode-converter system, greatly contribute to the discrepancy between the measured and the simulated field pattern at the final beam location (after the mode converter). This suggests that there is limited CCF dependency on whether the mode generator is rotating or non-rotating.

IV. CONCLUSIONS

In this paper, we demonstrated that our proposed cold-test scheme using a NRMG is a simple, efficient method for testing the quality of a QOMC design. To verify the proposed test scheme, we used a high-order linear $TE_{6,2}$ mode generator and benchmarked the results against those from a $TE_{6,2}$ RMG. Three different mode-converter test systems were

considered: an optimized dimpled launcher, an un-optimized dimpled launcher, and an un-optimized smooth launcher. The experimental results from the three mode-converter systems were compared to the simulation results. These results indicated that the field patterns of simulation and experimental data show excellent agreement, with cross-correlation values greater than 95%, even when using a NRMG. We find almost no difference in terms of the mode-converted quality when using the NRMG compared to the RMG. Furthermore, when non-ideal experimental conditions are included, the experimental results are in much better agreement with the simulation results, with cross-correlation values as high as 98%. Therefore, for cold testing mode converters, a higher-order NRMG may be preferable because it is much easier to design, fabricate, and test, and comprises a much more compact system than a higher-order RMG. In other words, typical mode converter tests using higher-order RMGs require time-consuming alignment processes, bulky systems, and the possibility of unwanted modes, and our study thus offers a more practical method for testing higher-frequency gyrotron devices.

ACKNOWLEDGMENTS

This research was supported by the National R&D Program through the National Research Foundation of Korea (NRF) funded by the Ministry of Science, ICT & Future Planning (Grant No. 2013R1A1A2061062) and by the Agency for Defense Development (ADD).

[1]M. Thumm, "Progress in gyrotron development," Fusion Eng. Des. **66–68**, 69–90 (2003).
[2]B. L. Smith and M. H. Carpentier, *The Microwave Engineering Handbook* (Chapman & Hall, London, 2003).
[3]M. Thumm, *State-of-the-Art of High Power Gyro-Devices and Free Electron Masers Update 2002* (FZK Internal Report, 2003).
[4]A. V. Gaponov, M. I. Petelin, and V. K. Yulpatov, Radiophys. Quantum Electron. **10**, 794–813 (1967).
[5]K. Sakamoto, A. Kasugai, K. Takahashi, R. Minami, N. Kobayashi, and K. Kajiwara, Nat. Phys. **3**, 411–414 (2007).
[6]M. K. Hornstein, V. S. Bajaj, R. G. Griffin, and R. J. Temkin, IEEE Trans. Plasma Sci. **34**, 524–533 (2006).
[7]A. C. Torrezan, S. T. Han, M. A. Shapiro, J. R. Sirigiri, and R. J. Temkin, IEEE Trans. Plasma Sci. **38**, 1150–1159 (2010).
[8]M. Thumm, Int. J. Infrared Milli. **26**, 483–503 (2005).
[9]E. A. Nanni, A. B. Barnes, R. G. Griffin, and R. J. Temkin, IEEE Trans. Terahz. Sci. Tech. **1**, 145–163 (2011).
[10]Y. Bykov, A. Eremeev, M. Glyavin, V. Kholoptsev, A. Luchinin, I. Plotnikov, G. Denisov, A. Bogdashev, G. Kalynova, V. Semenov, and N. Zharova, IEEE Trans. Plasma Sci. **32**, 67–72 (2004).
[11]B. Piosczyk, G. Dammertz, O. Dumbrajs, O. Drumm, S. Illy, J. Jin, and M. Thumm, IEEE Trans. Plasma Sci. **32**, 413–417 (2004).
[12]K. E. Kreischer and R. J. Temkin, Phys. Rev. Lett. **59**, 547–550 (1987).
[13]M. E. Read, G. S. Nusinovich, O. Dumbrajs, H. Q. Dinh, D. Opie, G. Bird, K. Kreischer, and M. Blank, IEEE Trans. Plasma Sci. **24**, 586–595 (1996).
[14]M. P. Perkins, R. Cao, J. M. Neilson, and R. J. Vernon, Int. J. Infrared Milli. **28**, 207–218 (2007).
[15]M. Blank, K. Kreischer, and R. J. Temkin, IEEE Trans. Plasma Sci. **24**, 1058–1066 (1996).
[16]R. Minami, A. Kasugai, K. Takahashi, N. Kobayashi, Y. Mitsunaka, and K. Sakamoto, Int. J. Infrared Milli. **27**, 13–24 (2006).
[17]J. M. Neilson and R. Bunger, IEEE Trans. Plasma Sci. **30**, 794–799 (2002).
[18]G. Li, J. Jin, T. Rzenicki, S. Kern, and M. Thumm, IEEE Trans. Plasma Sci. **38**, 1361–1368 (2010).
[19]D. S. Tax, E. M. Choi, I. Mastovsky, J. M. Neilson, M. A. Shapiro, J. R. Sirigiri, R. J. Temkin, and A. C. Torrezan, J. Infrared Mill. Terahz Waves **32**, 358–370 (2011).
[20]H. O. Prinz, A. Arnold, G. Dammertz, K. Koppenburg, and M. Thumm, in *Proceedings of the International Conference on Infrared, Millimeter, and Terahertz Waves 2005, 19–23 September, Williamsburg* (IEEE, 2005), pp. 297–298.
[21]Surf3d computational Ver. 2.43, GUI Ver. 1.21 user manual, Lexam research.
[22]C. T. Iatrou, IEEE Trans. Plasma Sci. **24**, 596–605 (1996).
[23]G. S. Nusinovich, M. E. Read, O. Dumbrajs, and K. E. Kreischer, IEEE Trans. Electron Dev. **41**, 433–438 (1994).
[24]G. S. Nusinovich, *Introduction to the Physics of Gyrotrons* (Johns Hopkins, Baltimore, MD, 2004).
[25]K. Kim, M. S. Choe, W. S. Lee, J. H. So, and E. M. Choi, IEEE Trans. Plasma Sci. **42**, 937–943 (2014).
[26]M. S. Choe and E. M. Choi, Microw. Optic. Tech. Lett. **56**, 1648–1651 (2014).
[27]N. L. Aleksandrov, A. V. Chirkov, G. G. Denisov, D. V. Vinogradov, W. Kasparek, J. Pretterebner, and D. Wagner, Int. J. Infrared Milli. **13**, 1369–1385 (1992).
[28]A. Arnold, O. Prinz, D. Wagner, and M. Thumm, in *Proceedings of the International Conference on Infrared, Millimeter, and Terahertz Waves 2007, 2–9 September, Cardiff* (IEEE, 2007), pp. 434–435.